

Article

Deformed Shell Model Applications to Weak Interaction Processes

R. Sahu ^{1,*} , V. K. B. Kota ² and T. S. Kosmas ³ ¹ National Institute of Science and Technology, Palur Hills, Berhampur 761008, India² Physical Research Laboratory, Ahmedabad 380009, India; vkbkota@prl.res.in³ Division of Theoretical Physics, University of Ioannina, GR 45110 Ioannina, Greece; hkosmas@uoi.gr

* Correspondence: rankasahu@gmail.com

Abstract: The deformed shell model (DSM), based on Hartree–Fock intrinsic states with angular momentum projection and band mixing, has been found to be quite successful in describing many spectroscopic properties of nuclei in the $A = 60$ – 100 region. More importantly, DSM has been used recently with good success in calculating nuclear structure factors, which are needed for a variety of weak interaction processes. In this article, in addition to giving an overview of this, we discuss the applications of DSM to obtain cross-sections for coherent and incoherent neutrino nucleus scattering on $^{96,98,100}\text{Mo}$ targets and also for obtaining two neutrino double beta decay nuclear transition matrix elements for ^{100}Mo .

Keywords: deformed shell model; $^{96,98,100}\text{Mo}$; coherent and incoherent neutrino nucleus scattering

1. Introduction

Over the last many years, the deformed shell model (DSM), based on Hartree–Fock intrinsic states with angular momentum projection and band mixing, has been established to be a good model to describe the properties of medium-mass nuclei—see the book [1] for details of DSM and for a summary of some of the applications of the model. DSM calculations are performed in the spirit of a spherical shell model, where one takes a model space and a suitable effective interaction (single-particle orbitals, single-particle energies, and a two-body effective interaction). This procedure has been found to be quite successful in the mass region $A = 60$ – 100 in describing spectroscopic properties like band crossing, shape coexistence, electro-magnetic transition probabilities, $T = 0$ and $T = 1$ bands in $N = Z$ odd–odd nuclei with isospin projection, and so on [1]. Going beyond spectroscopy, DSM has also been employed quite successfully for obtaining nuclear structure factors, which are needed for a variety of weak processes. These include (i) both two-neutrino and neutrinoless double beta decay, including positron double beta decay (all the examples studied so far are reviewed in [1]); (ii) $\mu \rightarrow e$ conversion in the field of the nucleus in ^{72}Ge [2]; (iii) event rates for WIMP nucleus scattering off ^{23}Na , ^{40}Ar , $^{71,73}\text{Ge}$, ^{75}As , ^{127}I , ^{133}Cs , and ^{133}Xe nuclei [3–6]; (iv) coherent and incoherent event rates for the neutrino-nucleus scattering from ^{28}Si , $^{64,70}\text{Zn}$, $^{70,71,73,76}\text{Ge}$, ^{75}As , ^{127}I , ^{133}Cs , and ^{133}Xe [4,5,7,8]. In the present paper, results are presented for neutrino-nucleus scattering cross-sections and two-neutrino double beta decay nuclear matrix elements obtained using DSM and involving Mo isotopes. Now, we give a preview.

In Section 2, we present some of the important steps in the formulation of DSM. In Section 3, we discuss its application to neutrino-nucleus scattering in $^{96,98,100}\text{Mo}$ isotopes. In Section 4, the application of the model to 2ν double beta decay in ^{100}Mo is presented. Finally, Section 5 gives conclusions.

2. Deformed Shell Model

The details of this model have been described in many of our earlier publications (see, for example, ref. [1]). In this model, for a given nucleus, starting with a model space



Citation: Sahu, R.; Kota, V.K.B.; Kosmas, T.S. Deformed Shell Model Applications to Weak Interaction Processes. *Particles* **2024**, *7*, 595–602. <https://doi.org/10.3390/particles7030033>

Academic Editor: Valery E. Lyubovitskij

Received: 3 June 2024

Revised: 26 June 2024

Accepted: 27 June 2024

Published: 29 June 2024



Copyright: © 2024 by the authors. Licensee MDPI, Basel, Switzerland. This article is an open access article distributed under the terms and conditions of the Creative Commons Attribution (CC BY) license (<https://creativecommons.org/licenses/by/4.0/>).

consisting of a given set of single-particle (sp) orbitals and effective two-body Hamiltonian (TBME + spe), the lowest-energy intrinsic states are obtained by solving the axially symmetric Hartree–Fock (HF) single-particle equation self-consistently. Excited intrinsic configurations are obtained by making particle–hole excitations over the lowest intrinsic state. These intrinsic states $\chi_K(\eta)$ do not have definite angular momenta. Hence, states of good angular momentum projected from an intrinsic state $\chi_K(\eta)$ can be written in the form

$$\psi_{MK}^J(\eta) = \frac{2J+1}{8\pi^2\sqrt{N_{JK}}} \int d\Omega D_{MK}^{J*}(\Omega) R(\Omega) |\chi_K(\eta)\rangle \tag{1}$$

where N_{JK} is the normalization constant, given by

$$N_{JK} = \frac{2J+1}{2} \int_0^\pi d\beta \sin \beta d_{KK}^J(\beta) \langle \chi_K(\eta) | e^{-i\beta J_y} | \chi_K(\eta) \rangle \tag{2}$$

In Equation(1), Ω represents the Euler angles (α, β, γ) and $R(\Omega)$, which is equal to $\exp(-i\alpha J_z) \exp(-i\beta J_y) \exp(-i\gamma J_z)$, represents the general rotation operator.

The good angular momentum states projected from different intrinsic states are not, in general, orthogonal to each other. Hence, they are orthonormalized and then band-mixing calculations are performed. The resulting eigenfunctions are of the form

$$|\Phi_M^J(\eta)\rangle = \sum_{K,\alpha} S_{K\eta}^J(\alpha) |\psi_{MK}^J(\alpha)\rangle. \tag{3}$$

3. Cross-Sections of Neutral-Current Neutrino Scattering on ^{96,98,100}Mo Isotopes

Some years ago, the neutral-current neutrino-nucleus channel was detected for the first time in the COHERENT experiment [9], more than four decades after its theoretical prediction by Freedman [10]. The measurement of coherent elastic event rates of neutrino scattering on a sodium-doped CsI detector may help in answering some key questions related to neutrino properties and provide an understanding of some theories beyond the standard model of the electroweak interactions [11]. Several promising nuclear detectors are on their way to being employed in designed and ongoing experiments [12–22]. Following all these, very recently, cross-sections for neutrino scatterings off ^{98,100}Mo were calculated by us, using DSM for nuclear structure factors [23]. In addition to briefly describing these results, here, we also report the first results for ⁹⁶Mo.

The details of the relevant formulation that provides the neutral-current ν -nucleus scattering differential cross-sections have been discussed earlier in [24–26]. Applying a multipole analysis on the weak Hadronic current [25,26], the neutrino-nucleus scattering cross-section becomes

$$\frac{d^2\sigma_{i\rightarrow f}}{d\Omega d\omega}(\phi, \theta, \omega, \epsilon_i) = \delta(E_f - E_i - \omega) \frac{2G^2\epsilon_f^2 \cos^2(\theta/2)}{\pi(2J_i + 1)} [C_V + C_A \mp C_{VA}] \tag{4}$$

The δ -function on the right-hand side of the above equation ensures the energy conservation, so that the excitation energy of the nucleus ω is given by

$$\omega = E_f - E_i = \epsilon_i - \epsilon_f \tag{5}$$

E_i and E_f represent the energy of the initial and final states of the studied nucleus, and ϵ_i and ϵ_f are the incoming and outgoing energies of the neutrino. In Equation (4), the $(-)$ sign corresponds to the scattering of the neutrinos and the $(+)$ to the scattering of the antineutrinos.

The terms C_V and C_A include a summation over the contributions coming from the polar-vector and axial-vector multipole operators. Similarly, the interference term C_{VA} in Equation (4) contains the product of transverse polar-vector and transverse axial-vector matrix elements. All these involve square of the four-momentum transfer q_μ^2 and the scattering

angle θ . Note that the square of the four-momentum transfer q_μ^2 and the magnitude of the three-momentum transfer $q \equiv |\mathbf{q}|$ can be written in terms of the kinematic parameters, i.e., laboratory scattering angle θ and neutrino energies $\epsilon_i = \epsilon_\nu$ and $\epsilon_f = (\epsilon_i - \omega)$, as

$$\begin{aligned} q_\mu^2 &\equiv q_\mu q^\mu = -4\epsilon_i(\epsilon_i - \omega) \sin^2(\theta/2) \\ q &\equiv |\mathbf{q}| = [\omega^2 + 4\epsilon_i(\epsilon_i - \omega) \sin^2(\theta/2)]^{1/2} \end{aligned} \quad (6)$$

The reduced matrix elements that enter in the formulas for $C_{V(A)}$ and C_{VA} are evaluated using DSM band-mixed wave function $\Phi_M^J(\eta)$, defined in Equation (3). Full details of the various operators and the method employed for the calculation of various reduced matrix elements are given in [23].

In the calculations for $^{96,98,100}\text{Mo}$ isotopes, we have adopted the effective interaction *GWBXG* with the ^{66}Ni as the closed core. The details regarding the construction of the effective interaction have been discussed in refs. [27,28]. The active proton orbits are $0f_{5/2}$, $1p_{3/2}$, $1p_{1/2}$, and $0g_{9/2}$ with single-particle energies -5.322 , -6.144 , -3.941 , and -1.250 MeV. For the neutrons, the active orbits are $1p_{1/2}$, $0g_{9/2}$, $0g_{7/2}$, $1d_{5/2}$, $1d_{3/2}$, and $2s_{1/2}$. The single-particle energies for the first five orbits are taken to be -0.696 , -2.597 , 5.159 , 1.830 , and 4.261 MeV, respectively. The $2s_{1/2}$ orbit produces low-lying large deformed solutions, even though molybdenum isotopes are known to be weakly deformed. Hence, the effect of this orbit is eliminated by taking the corresponding neutron single-particle energy at a high value.

Using the above effective interaction and the single-particle energies, we first carried out an axially symmetric HF calculation by solving the HF equation self-consistently. The detailed spectroscopic results obtained using DSM for ^{98}Mo and ^{100}Mo are given in [23]. The observed low-lying energy levels for both the nuclei are well-reproduced in our calculation, as are the lowest few $B(E2)$ values. Beyond these two isotopes, here, we report briefly the results obtained for ^{96}Mo . For ^{96}Mo , the axially symmetric HF calculation is carried out using the above-described model space and effective interaction. It is found that the lowest prolate and oblate HF solutions are almost degenerate, with the oblate solution being lower by ~ 0.25 MeV. We obtained excited HF configurations by making particle-hole excitations over these lowest HF configurations. For positive parity, we consider 33 intrinsic configurations (17 oblate and 16 prolate) and, for negative parity, 24 intrinsic configurations (12 oblate and 12 prolate). As described before, good angular momentum states are projected from each of these intrinsic states. These states are not orthogonal to each other. Hence, they are orthonormalized and a band-mixing calculation is performed. States having similar structure and, thus, similar electromagnetic properties are classified in one band. For ^{96}Mo , not many collective bands have been observed. In Figure 1, we compare the calculated ground band with the experimentally observed band and we see that the agreement is reasonable. Further details regarding other spectroscopic properties of ^{96}Mo will be reported elsewhere.

One of our goals is to calculate the incoherent differential cross-sections for each J^π state of Mo isotopes with $A = 92-100$. Here, we report some results for $^{96,98,100}\text{Mo}$ isotopes and they are obtained by evaluating the transition matrix elements, defining C_V , C_A and C_{VA} , and connecting the ground 0^+ state to various excited J^π states through the use of the DSM wave function $\Phi_M^J(\eta)$ defined in Equation (3). The incoming neutrino energy is assumed to be $\epsilon_\nu = 15$ MeV. We use a quenching factor of 0.35. Results for $^{98,100}\text{Mo}$ are given in our recent publication [23] and they are summarized in Figure 2. In addition, recently, we have also considered neutrino scattering off ^{96}Mo and details of this study will be presented in a separate publication. Here, we summarize, in Table 1, the calculated ratio of the coherent to the total (coherent + incoherent) cross-section for the three Mo isotopes. These lie, as seen from Table 1, between 85% and 91%. We note that our cross-sections correspond only to the Standard Model (SM) ν -nucleus interactions. It is worth remarking that, in other BSM electroweak processes where the coherent channel is also possible,

e.g., the muon-to-electron conversion in nuclei (see e.g., refs. [29,30]), the portion of the coherent branching ratio into the total one represents also about 85–90 % of the total rate.

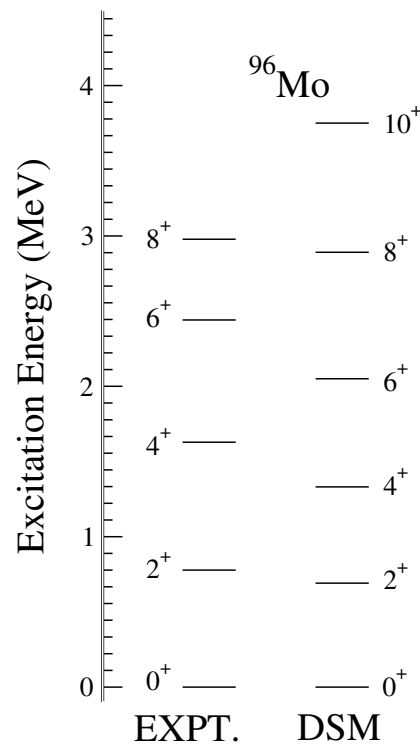


Figure 1. The ground band observed for ^{96}Mo is compared with the DSM predicted values. The experimental data are taken from [31].

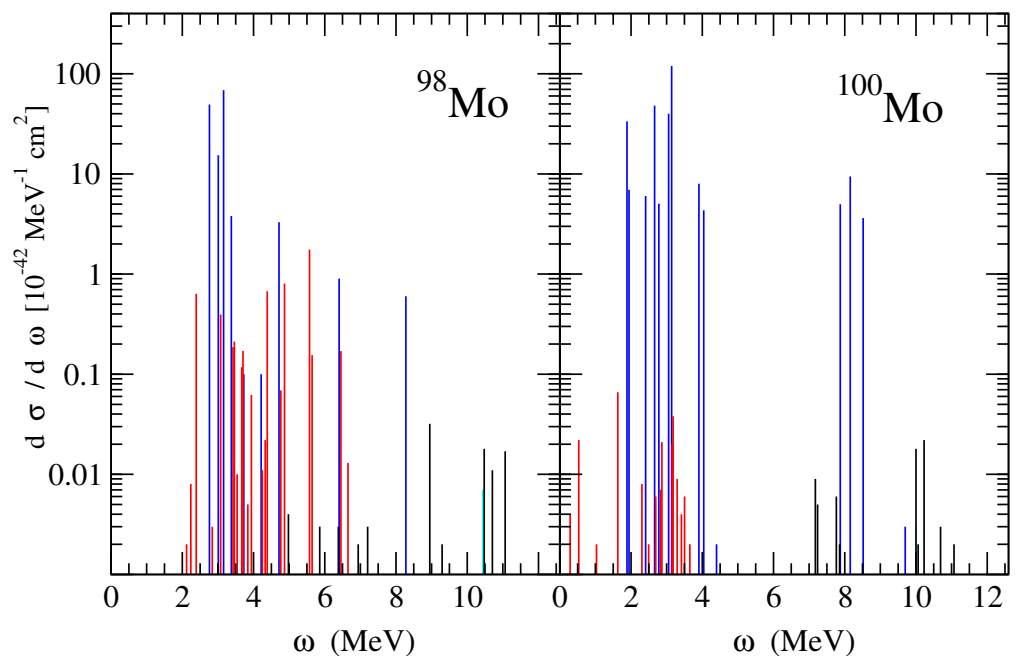


Figure 2. The differential cross-section as a function of the excitation energy ω for $^{98,100}\text{Mo}$ at incoming neutrino energy $\epsilon_\nu = 15 \text{ MeV}$ for different excited states. The data are taken from ref. [23]. The contribution of the excitation to the $J = 1^+$ state is represented by blue, to $J = 2^+$ by red, to $J = 1^-$ by cyan, and to $J = 2^-$ by black.

Table 1. Coherent, incoherent, and total differential cross-sections (in units of $10^{-42} \text{ MeV}^{-1} \text{ cm}^2$) of neutrino scattering off the $^{96,98,100}\text{Mo}$ detector isotopes. The portion of the coherent into the total cross-section is also listed. Results for $^{98,100}\text{Mo}$ are taken from [23].

Isotope	Coherent	Incoherent	Total	Coherent/Total (%)
^{96}Mo	1338.5	230.0	1568.5	85.34 (%)
^{98}Mo	1506.2	147.7	1653.9	91.07 (%)
^{100}Mo	1692.9	290.0	1982.9	85.38 (%)

4. 2ν Double Beta Decay of ^{100}Mo

The two-neutrino double beta decay ($2\nu\text{DBD}$) is a second-order process of weak interaction. This decay has been observed in more than 10 nuclei and is consistent with the standard model. On the other hand, neutrinoless double beta decay violates lepton number conservation and has not been observed. The successful description of the half-lives (or nuclear matrix elements) for $2\nu\beta\beta$ decay provides a stringent test of the goodness of the nuclear model used, and, with confidence, we can use it to predict the neutrinoless double beta decay matrix elements. A number of nuclear models has been used to study $2\nu\text{DBD}$, namely, spherical shell model [28,32–34], QRPA and its variants [35], interacting boson model [36], deformed shell model [1], and so on. Recently, Patel et al. [34] have employed large-scale shell model calculations to study the two-neutrino double beta decay in ^{82}Se , ^{94}Zr , ^{108}Cd , ^{124}Sn , ^{128}Te , ^{130}Te , ^{136}Xe , and ^{150}Nd using different effective interactions. Deformed shell model calculations have been performed to study the double beta decay for different nuclei in the $A = 60\text{--}90$ region and the results have been summarized in ref. [1]. The nucleus ^{100}Mo is a famous double beta decay emitter and has been employed in various experiments like NEMO [37] and MOON [38]. Different variants of QRPA have been used to study $\beta\beta$ decay for this nucleus [39]. But there are very few shell model calculations for this nucleus because of the large matrices to be diagonalized. Recently, Coraggio et al [33] have performed shell model calculation for this nucleus using effective $2\nu\beta\beta$ operators. Here, we discuss the application of DSM for two-neutrino double beta decay of ^{100}Mo ($0\nu\beta\beta$ decay will be considered elsewhere).

Half-life for the $0_i^+ \rightarrow 0_f^+ 2\nu\text{DBD}$ is given by

$$\left[T_{1/2}^{2\nu}\right]^{-1} = G_{2\nu} g_A^4 |M_{2\nu}|^2 \tag{7}$$

g_A corresponds to the axial-vector coupling constant. The kinematical factor $G_{2\nu}$ is independent of nuclear structure and its value $G_{2\nu} = 310.6 \times 10^{-20} \text{ yr}^{-1}$ [40]. On the other hand, the nuclear transition matrix elements (NTME) $M_{2\nu}$ are nuclear-model-dependent and they are given by

$$M_{2\nu} = \sum_m \frac{\langle 0_f^+ || \sigma \tau^+ || 1_m^+ \rangle \langle 1_m^+ || \sigma \tau^+ || 0_i^+ \rangle}{\left[E_m - (E_i + E_f)/2\right] / m_e} \tag{8}$$

where $|0_i^+\rangle$, $|0_f^+\rangle$, and $|1_m^+\rangle$ are the initial, final, and virtual intermediate states, respectively, and E_m are the energies of the intermediate nucleus ^{100}Tc . Similarly, E_i and E_f are the ground-state energies of the parent and daughter nuclei. We have, from ref. [41], the atomic masses of ^{100}Mo , ^{100}Tc , and ^{100}Ru as -86.193 , -86.0215 , and -89.227 MeV , respectively (for nuclear mass, we need to subtract the mass of the electrons from the atomic mass). Experimentally, the lowest 1^+ state in ^{100}Tc is the ground state. We finally obtain $[E_m - (E_i + E_f)/2] = [1.689 + E_{1^+}] \text{ MeV}$. DSM is used to calculate the energies E_{1^+} of the 1^+ states of ^{100}Tc and the corresponding wave functions. Similarly, we obtained ground-state (with 0^+) wave functions of ^{100}Mo and the daughter nucleus ^{100}Ru . With these, the reduced matrix elements in Equation (8) are obtained. We have included 29 1^+ states

(up to 5.7 MeV) in the calculation. The calculated half life is compared with experiments in Table 1 and the calculated half life is about 20 times larger compared to the experimental value. Employing the renormalized GT operator or, equivalently, using an effective g_A value, as mentioned in Table 2, will improve the calculated half life, just as in the shell model [33].

Table 2. DSM-calculated $2\nu\beta\beta$ decay half lives for ^{100}Mo with $g_A = 1$. With axial vector coupling constant $g_A = 1.267$, half life becomes 5.26×10^{19} (yr). Experimental value is taken from [42].

J_f	$M_{2\nu}$	$G_{2\nu}$	Calculated $T_{1/2}^{2\nu}$	Expt. Value
0^+	0.049	3.106×10^{-18} (yr $^{-1}$)	1.35×10^{20} (yr)	$7.06_{-0.13}^{+0.15} \times 10^{18}$ (yr)

5. Conclusions

We have described the application of DSM to evaluate incoherent and coherent cross-sections for $^{96,98,100}\text{Mo}$. As a test of DSM, we have also reported the half life for two neutrino double beta decays of ^{100}Mo and compared them with experimental values. The recently observed neutral-current coherent elastic neutrino-nucleus scattering data, as well as those expected to be measured at the designed CE ν NS experiments with other nuclear detectors, offer the possibility to constrain the parameter space of several models, progressing beyond the standard model, which assumes vector and scalar mediators. Our present predictions on the $^{96,98,100}\text{Mo}$ may be of help towards this direction since, as is known, these isotopes are prominent detection media. They have been employed previously in appreciably sensitive detectors (for the detection of neutrinoless double beta decay and dark matter) in the MOON and NEMO experiments.

Finally, it may be useful to perform DSM calculations for nuclear structure factors with an improved effective interactions and also by including many more deformed intrinsic states. This will be attempted in the future.

Author Contributions: All the authors contributed equally. All authors have read and agreed to the published version of the manuscript.

Funding: This research was funded by Association for Advancement of Research on Open Problems (OPRA Association, Tel Aviv, Israel) in Nuclear Physics & Particle Physics, project No 83241/ELKE-UoI. And SERB in the Department of Science and Technology (Government of India) for financial support.

Data Availability Statement: All the numerical data for generating Figures and Tables of the paper can be obtained from the first author R. Sahu.

Acknowledgments: Thanks are due to P. C. Srivastava for some useful correspondence.

Conflicts of Interest: The authors declare no conflict of interest.

References

- Kota, V.K.B.; Sahu, R. *Structure of Medium Mass Nuclei: Deformed Shell Model and Spin-Isospin Interacting Boson Model*; CRC Press: Boca Raton, FL, USA; Taylor & Francis Group: Boca Raton, FL, USA, 2017.
- Kosmas, T.S.; Faessler, A.; Sahu, R. Transition matrix elements for $\mu \rightarrow e$ conversion in ^{72}Ge using the deformed Hartree Fock method. *Phys. Rev. C* **2003**, *68*, 054315. [CrossRef]
- Sahu, R.; Kota, V.K.B. Deformed shell model study of event rates for WIMP- ^{73}Ge scattering. *Mod. Phys. Lett. A* **2017**, *32*, 1750210. [CrossRef]
- Papoulias, D.K.; Sahu, R.; Kosmas, T.S.; Kota, V.K.B.; Nayak, B. Novel neutrino-floor and dark matter searches with deformed shell model calculations. *Adv. High Energy Phys.* **2018**, *2018*, 6031362. [CrossRef]
- Sahu, R.; Papoulias, D.K.; Kota, V.K.B.; Kosmas, T.S. Elastic and inelastic scattering of neutrinos and weakly interacting massive particles on nuclei. *Phys. Rev. C* **2020**, *102*, 035501. [CrossRef]
- Sahu, R.; Kota, V.K.B.; Kosmas, T.S. Event rates for the scattering of weakly interacting massive particles from ^{23}Na and ^{40}Ar . *Particles* **2021**, *4*, 75. [CrossRef]
- Papoulias, D.K.; Kosmas, T.S.; Sahu, R.; Kota, V.K.B.; Hota, M. Constraining nuclear physics parameters with current and future COHERENT data. *Phys. Lett. B* **2020**, *800*, 135133. [CrossRef]

8. Kosmas, T.S.; Kota, V.K.B.; Papoulias, D.K.; Sahu, R. Coherent elastic neutrino-nucleus scattering (*CEvNS*) event rates for Ge, Zn, and Si detector materials. *Phys. Rev. C* **2021**, *104*, 064618. [[CrossRef](#)]
9. Akimov, D.; Albert, J.B.; An, P.; Awe, C.; Barbeau, P.S.; Becker, B.; Belov, V.; Brown, A.; Bolozdynya, A.; Cabrera-Palmer, B.; et al. Observation of Coherent Elastic Neutrino-Nucleus Scattering. *Science* **2017**, *357*, 1123. [[CrossRef](#)]
10. Freedman, D.Z. Coherent effects of a weak neutral current. *Phys. Rev. D* **1974**, *9*, 1389. [[CrossRef](#)]
11. Papoulias, D.K.; Kosmas, T.S. COHERENT constraints to conventional and exotic neutrino physics. *Phys. Rev. D* **2018**, *97*, 033003. [[CrossRef](#)]
12. Colaresi, J.; Collar, J.; Hossbach, T.; Lewis, C.; Yocum, K. Measurement of Coherent Elastic Neutrino-Nucleus Scattering from Reactor Antineutrinos. *Phys. Rev. Lett.* **2022**, *129*, 211802. [[CrossRef](#)]
13. CONNIE Collaboration; Aguilar-Arevalo, A.; Bernal, J.; Bertou, X.; Bonifazi, C.; Cancelo, G.; de Carvalho, V.G.P.B.; Cervantes-Vergara, B.A.; Chavez, C.; Corrêa, G.C.; et al. Search for coherent elastic neutrino-nucleus scattering at a nuclear reactor with CONNIE 2019 data. *JHEP* **2022**, *05*, 017.
14. Bonet, H.; Bonhomme, A.; Buck, C.; Fülber, K.; Hakenmüller, J.; Heusser, G.; Hugle, T.; Lindner, M.; Maneschg, W.; Rink, T.; et al. Novel constraints on neutrino physics beyond the standard model from the CONUS experiment. *JHEP* **2022**, *05*, 085.
15. Alekseev, I.; Balej, K.; Belov, V.; Evseev, S.; Filosofov, D.; Fomina, M.; Hons, Z.; Karaivanov, D.; Kazartsev, S.; Khushvaktov, J.; et al. First results of the ν GeN experiment on coherent elastic neutrino-nucleus scattering. *Phys. Rev. D* **2022**, *106*, L051101. [[CrossRef](#)]
16. Agnolet, G.; Baker, W.; Barker, D.; Beck, R.; Carroll, T.J.; Cesar, J.; Cushman, P.; Dent, J.B.; Rijck, S.D.; Dutta, B.; et al. Background Studies for the MINER Coherent Neutrino Scattering Reactor Experiment. *Nucl. Instrum. Meth. A* **2017**, *853*, 53. [[CrossRef](#)]
17. Billard, J.; Carr, R.; Dawson, J.; Figueroa-Feliciano, E.; Formaggio, J.A.; Gascon, J.; Jesus, M.D.; Johnston, J.; Lasserre, T.; Leder, A.; et al. Coherent Neutrino Scattering with Low Temperature Bolometers at Chooz Reactor Complex. *J. Phys. G* **2017**, *44*, 105101. [[CrossRef](#)]
18. Strauss, R.; Rothe, J.; Angloher, G.; Bento, A.; Gütlein, A.; Hauff, D.; Kluck, H.; Mancuso, M.; Oberauer, L.; Petricca, F.; et al. The ν -cleus experiment: A gram-scale fiducial-volume cryogenic detector for the first detection of coherent neutrino-nucleus scattering. *Eur. Phys. J. C* **2017**, *77*, 506. [[CrossRef](#)]
19. Wong, H.T.-K. Taiwan Experiment On Neutrino: History and Prospects. *Universe* **2015**, *3*, 22. [[CrossRef](#)]
20. Augier, C.; Baulieu, G.; Belov, V.; Bergé, L.; Billard, J.; Bres, G.; Bret, J.-L.; Broniatowski, A.; Calvo, M.; Cazes, A.; et al. Results from a Prototype TES Detector for the Ricochet Experiment. *arXiv* **2023**, arXiv:2304.14926v1.
21. Fernandez-Moroni, G.; Machado, P.A.N.; Martinez-Soler, I.; Perez-Gonzalez, Y.F.; Rodrigues, D.; Rosauero-Alcaraz, S. The physics potential of a reactor neutrino experiment with Skipper CCDs: Measuring the weak mixing angle. *JHEP* **2021**, *03*, 186. [[CrossRef](#)]
22. Flores, L.J.; Peinado, E.; Alfonso-Pita, E.; Allen, K.; Baker, M.; Behnke, E.; Bressler, M.; Clark, K.; Coppejans, R.; Cripe, C.; et al. Physics reach of a low threshold scintillating argon bubble chamber in coherent elastic neutrino-nucleus scattering reactor experiments. *Phys. Rev. D* **2021**, *103*, L091301. [[CrossRef](#)]
23. Sahu, R.; Kota, V.K.B.; Kosmas, T.S. Cross sections of neutral-current neutrino scattering on $^{98,100}\text{Mo}$ isotopes. *J. Phys. G Nucl. Part. Phys.* **2024**, *51*, 065104 [[CrossRef](#)]
24. Tsakstara, V.; Kosmas, T.S. Low-energy neutral-current neutrino scattering on $^{128,130}\text{Te}$ isotopes. *Phys. Rev. C* **2011**, *83*, 054612. [[CrossRef](#)]
25. Donnelly, T.W.; Walecka, J.D. Semi-leptonic weak and electromagnetic interactions with nuclei: Isoelastic processes. *Nucl. Phys. A* **1976**, *274*, 368. [[CrossRef](#)]
26. Donnelly, T.W.; Peccei, R.D. Neutral current effects in nuclei. *Phys. Rep.* **1979**, *50*, 1. [[CrossRef](#)]
27. Dey, P.; Negi, D.; Palit, R.; Srivastava, P.C.; Laskar, M.S.R.; Das, B.; Babra, F.S.; Bhattacharya, S.; Das, B.; Devi, K.R.; et al. Experimental investigation of high-spin states in ^{90}Zr . *Phys. Rev. C* **2022**, *105*, 044307. [[CrossRef](#)]
28. Coraggio, L.; De Angelis, L.; Fukui, T.; Gargano, A.; Itaco, N. Calculation of Gamow-Teller and two-neutrino double- β decay properties for ^{130}Te and ^{136}Xe with a realistic nucleon-nucleon potential. *Phys. Rev. C* **2018**, *59*, 064324.
29. Kosmas, T.S.; Faessler, A.; Vergados, J.D. The new limits of the neutrinoless (μ^- , e^-) conversion branching ratio. *J. Phys. G: Nucl. Part. Phys.* **1997**, *23*, 693. [[CrossRef](#)]
30. Kosmas, T.S. Current Nuclear Physics Issues in Studying the Neutrinoless (μ^- , e^-) Conversion in Nuclei. *Prog. Part. Nucl. Phys.* **2002**, *48*, 307. [[CrossRef](#)]
31. Available online: <http://www.nndc.bnl.gov/> (accessed on 26 June 2024).
32. Kostensalo, J.; Suhonen, J.; Zuber, K. The first large-scale shell-model calculation of the two-neutrino double beta decay of ^{76}Ge to the excited states in ^{76}Se . *Phys. Lett. B* **2022**, *831*, 137170. [[CrossRef](#)]
33. Coraggio, L.; Itaco, N.; De Gregorio, G.; Gargano, A.; Mancino, R.; Nowacki, F. Shell-model calculation of ^{100}Mo double- β decay. *Phys. Rev. C* **2022**, *105*, 034312. [[CrossRef](#)]
34. Patel, D.; Srivastava, P.C.; Kota, V.K.B.; Sahu, R. Large-scale shell-model study of two-neutrino double beta decay of ^{82}Se , ^{94}Zr , ^{108}Cd , ^{124}Sn , ^{128}Te , ^{130}Te , ^{136}Xe , and ^{150}Nd . *Nucl. Phys. A* **2024**, *1042*, 122808. [[CrossRef](#)]
35. Yousef, M.S.; Rodin, V.; Faessler, A.; Simkovic, F. Two-neutrino double β decay of deformed nuclei within the quasiparticle random-phase approximation with a realistic interaction. *Phys. Rev. C* **2009**, *79*, 014314. [[CrossRef](#)]
36. Nomura, K. Two-neutrino double- β decay in the mapped interacting boson model. *Phys. Rev. C* **2022**, *105*, 044301. [[CrossRef](#)]

37. Arnold, R.; Augier, C.; Baker, J.; Barabash, A.; Broudin, G.; Brudanin, V.; Caffrey, A.J.; Caurier, E.; Egorov, V.; Errahmane, K.; et al. First Results of the Search for Neutrinoless Double-Beta Decay with the NEMO 3 Detector. *Phys. Rev. Lett.* **2005**, *95*, 182302. [[CrossRef](#)]
38. Shima, T.; Doe, P.J.; Ejiri, H.; Elliot, S.R.; Engel, J.; Finger, M.; Finger, M., Jr.; Fushimi, K.; Gehman, V.M.; Greenfield, M.B.; et al. MOON for next-generation neutrino-less double-beta decay experiment; present status and perspective. *J. Phys. Conf. Ser.* **2008**, *120*, 052055. [[CrossRef](#)]
39. Bobyk, A.; Kamiński, W.A.; Zareba, P. Study of the double beta decay of $70 \leq A \leq 100$ nuclei within the RQRPA and the self-consistent BCS+RQRPA formalisms. *Nucl. Phys. A* **2000**, *669*, 221. [[CrossRef](#)]
40. Neacsu, A.; Horoi, M. An effective method to accurately calculate the phase space factors for $\beta^- \beta^-$ decay. *Adv. High Energy Phys.* **2016**, *2016*, 7486712. [[CrossRef](#)]
41. Wang, M.; Audi, G.; Kondevi, F.G.; Huang, W.J.; Naimi, S.; Xing, X. The AME2016 atomic mass evaluation (II). Tables, graphs and references. *Chin. Phys. C* **2017**, *41*, 030003. [[CrossRef](#)]
42. Barabash, A.S. Precise half-life values for two-neutrino double- β decay: 2020 review. *Universe* **2020**, *6*, 159. [[CrossRef](#)]

Disclaimer/Publisher's Note: The statements, opinions and data contained in all publications are solely those of the individual author(s) and contributor(s) and not of MDPI and/or the editor(s). MDPI and/or the editor(s) disclaim responsibility for any injury to people or property resulting from any ideas, methods, instructions or products referred to in the content.